nature materials

Review Article

https://doi.org/10.1038/s41563-022-01468-y

Controlling persistent luminescence in nanocrystalline phosphors

Received: 25 March 2022

Accepted: 16 December 2022

Published online: 2 March 2023

Check for updates

Liangliang Liang[1], Jiaye Chen[1], Kang Shao[2], Xian Qin[1], Zaifa Pan[2] ✉ & Xiaogang Liu[1,3,4] ✉

Persistent luminescent phosphors can store light energy in advance and release it with a long-lasting afterglow emission. With their ability to eliminate in situ excitation and store energy for long periods of time, they are promising for broad applications, including background-free bioimaging, high-resolution radiography, conformal electronics imaging and multilevel encryption. This Review provides an overview of various strategies for trap manipulation in persistent luminescent nanomaterials. We highlight key examples in the design and preparation of nanomaterials with tunable persistent luminescence, particularly in the near-infrared range. In subsequent sections, we cover the most current developments and trends concerning the use of these nanomaterials in biological applications. Moreover, we assess their advantages and disadvantages compared with conventional luminescent materials for biological applications. We also discuss future research directions and challenges, such as insufficient brightness at the single-particle level, and possible solutions to these challenges.

Persistent luminescence is an optical process by which luminescent materials emit light for minutes or even hours after excitation ceases. Its mystical properties, first documented in the early 17th century, have fascinated researchers ever since[1–3]. Recently, various persistent luminescent phosphors at the nanoscale, such as $ZnGa_2O_4:Cr^{3+}$ and lanthanide-doped fluorides, have been explored[4–6]. The delayed emission of persistent luminescent nanophosphors and their small physical dimensions make them highly desirable for applications ranging from optical data storage to medical imaging and biological applications[7–9]. Compared with conventional organic dyes and quantum dots, persistent luminescent phosphors enable long-term luminescence detection without in situ excitation, which attenuates autofluorescence[10]. Suppression of background noise drastically improves detection sensitivity and image resolution for bioimaging. Moreover, downscaling phosphors with proper surface functionalization to the nanoscale can improve colloidal stability and biocompatibility, increase cell targeting efficiency and expand bioapplication opportunities. More importantly, light attenuation and scattering in the optical window are markedly reduced, making near-infrared persistent luminescent nanomaterials attractive for deep-tissue imaging.

Persistent luminescence

In most photoluminescent events of organic systems, fluorescence occurs when a chemical entity in the excited state radiates energy through allowed optical transitions on a timescale of less than tens of nanoseconds[11]. Unlike transitions between excited singlet states and the ground state (S_0), phosphorescence is characterized by an intersystem crossing (ISC) to an energy state with higher spin multiplicity (T_1), resulting in delayed emission. The transition from T_1 to S_0 still occurs, although it is spin forbidden, but it usually occurs over hundreds of microseconds[12]. The design of molecular structures and control of aggregation behaviour can result in phosphorescence lasting hundreds of milliseconds or even tens of seconds at room temperature[13]. Furthermore, charge separation and recombination strategies have been used to generate hours-long persistent luminescence from organic systems[14–16]. The luminescence lifetime of inorganic phosphors is usually

[1]Department of Chemistry, National University of Singapore, Singapore, Singapore. [2]College of Chemical Engineering, Zhejiang University of Technology, Hangzhou, China. [3]Center for Functional Materials, National University of Singapore Suzhou Research Institute, Suzhou, China. [4]Institute of Materials Research and Engineering, Agency for Science, Technology and Research, Singapore, Singapore. ✉e-mail: panzaifa@zjut.edu.cn; chmlx@nus.edu.sg

https://doi.org/10.1038/s41563-022-01468-y

BOX 1

Principles of long persistent luminescence in inorganic and organic systems

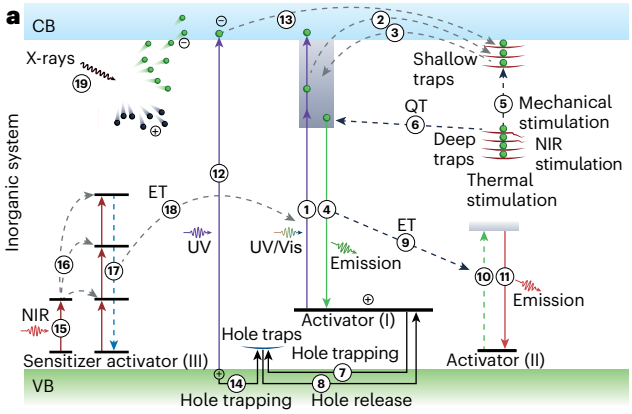

In an inorganic persistent luminescent system (**a**), the persistent luminescence process is typically initiated by direct excitation of doped activators or by transitions between the host valence band (VB) and conduction band (CB). The pumping source varies from low-energy excitation including by UV, visible and NIR, to high-energy ionizing irradiation such as by X-rays. Upon excitation, doped activators can be activated (step 1) so that electrons pumped to higher energy levels that overlap with the conduction band may diffuse to electron traps (step 2). However, not all trapping processes involve the conduction band. Shallowly trapped electrons can be easily transferred back to the conduction band at room temperature and then captured by activators to generate luminescence (steps 3 and 4). By contrast, deeply trapped electrons find escape relatively difficult. Before traps are emptied, persistent luminescence can usually be rejuvenated by external stimuli, such as heating, light irradiation and mechanical force (step 5).

Since the shallow-trap-based discharge is fast and sustains short persistent luminescence, a quantum tunnelling (QT) model for deeply trapped electrons has been proposed to explain the ultralong (tens of hours) persistent luminescence (step 6). Although electrons serve as primary charge carriers, hole traps could coexist with electron traps in most host matrices. Photoexcitation-induced holes in activators can be captured and released by hole traps via migration across the valence band (steps 7 and 8). Energy transfer (ET) between different types of emitters can be used to expand the spectrum of a given persistent luminescent phosphor (steps 9–11).

In addition to activators, the host matrix can usually be activated to generate electrons in the conduction band and holes in the valence band upon UV excitation (step 12). These charge carriers are subsequently captured by the corresponding traps (steps 13 and 14) and gradually released to doped activators (steps 3 and 8) to trigger persistent luminescence (step 4). Compared with visible light excitation, UV irradiation with a photon energy greater than the host bandgap usually induces much stronger persistent luminescence.

NIR-chargeable persistent luminescent systems can be constructed by integrating NIR-excitable up-conversion phosphors. With NIR illumination, up-conversion-integrated phosphors can be activated, and NIR photons absorbed by sensitizers (step 15) are up-converted and stored (step 16) in activators. Finally, the stored energy is transferred non-radiatively to persistent luminescent activators (steps 17 and 18), triggering persistent luminescence. Additionally, X-rays can produce abundant electron–hole pairs through the Auger effect and Compton scattering. These excitons can be trapped by defects such as colour centres to trigger persistent luminescence (step 19).

Hours-long persistent luminescence can also be achieved in organic systems (**b**(i)). As with the inorganic persistent luminescent system, photoactivation (step 1) of a blended organic donor/acceptor system can create photoinduced ionized states (step 2) and charge-separated states (step 3). Importantly, the long-lived charge-separated intermediate states can accumulate and diffuse throughout the matrix. Finally, the gradual recombination of the radical anions and radical cations generates an exciplex emission (step 4) through transitions from the lowest unoccupied molecular orbital (LUMO) of the acceptor to the highest occupied molecular orbital (HOMO) of the donor, producing hours-long persistent luminescence.

In addition, a generic approach has been developed to transform ordinary fluorescent agents into long-lasting luminescent nanoparticles, which relies on a cascade photoreaction within the particles to store energy (**b**(ii)). Upon excitation, a photosensitizer that serves as an initiator of persistent luminescence can be populated to its triplet states through (ISC) and then trigger the generation of singlet oxygen ($^1O_2$). Then, the singlet oxygen can be absorbed by a $^1O_2$-reactive molecular substrate to form an unstable chemiluminescent intermediate. Lastly, the energy of the intermediate can be gradually absorbed by a fluorescent agent, which works as a persistent luminescent relay unit through chemically initiated electron exchange, resulting in hours-long persistent luminescence.

measured in tens of nanoseconds for allowed electronic transitions (for example, $5d$–$4f$ in Ce^{3+})[17]; however, the lifetime can be prolonged to tens of milliseconds for parity-forbidden transitions (for example, f–f in Tb^{3+})[18]. For inorganic persistent luminescent phosphors, the ultra-slow persistent emission is induced by high-efficiency trapping and slow de-trapping of charge carriers, leading to tens of hours to days of persistent luminescence.

In recent decades, scientists have studied the origin of persistent luminescence in inorganic phosphors[19]. Although several theoretical models have been proposed, including electron trapping/discharge,

hole trapping/discharge and quantum tunnelling, it is likely that these processes coexist in many persistent luminescent systems (Box 1).

In principle, many kinds of crystal imperfections, such as vacancies, interstitial ions, impurities and dopants, can act as electron traps with a broad energy distribution in depth. Energy transfer has been widely used to achieve tunable luminescence in phosphors, especially to the near-infrared (NIR) region. As for the pumping source, ultraviolet–visible (UV–Vis) light is the most widely used source to charge persistent luminescent phosphors; however, persistent luminescent phosphors that can be charged with deep-red and even NIR light sources are highly desirable for biological applications. Lanthanide-based photon up-conversion has been developed to realize anti-Stokes emission upon NIR excitation. During the up-conversion process, incident low-energy photons are typically absorbed by lanthanide sensitizers and then transferred to proximal activators, followed by sequential populations in higher excited states[20]. Consequently, the activators emit high-energy photons in the UV–Vis region, which can be used to charge persistent luminescent phosphors. Importantly, X-rays have negligible scattering and a large penetration depth, making them an alternative source for persistent luminescence generation.

Trap manipulation for persistent luminescent phosphors

Intrinsic lattice point defects are widely considered responsible for charge carrier trapping, and multiple types of defects usually coexist in a phosphor (Fig. 1a). To illustrate, during material synthesis, cation and anion vacancies can be generated simultaneously in a stoichiometric ratio to maintain charge neutrality. These defects, termed Schottky defects, are randomly distributed in the host matrix. Meanwhile, ions can also migrate into interstitial sites, leaving vacancies to form Frenkel defects. In addition, antisite defects can form in weakly ionic compounds when cations and anions exchange positions. In addition to traps formed during synthesis, codoping with foreign ions has proven to be a practical approach to introducing traps that can greatly influence persistent luminescence. Many strategies have been explored to manipulate lattice defects, including aliovalent substitution, non-stoichiometric synthesis, lanthanide ion codoping and sintering atmosphere tuning. Beyond controlling the trap state by chemical means, persistent luminescence can be tuned by altering charging temperature and power. X-ray irradiation has also been shown to be efficient in creating electron/hole traps by displacing anions in lanthanide-activated fluorides.

Aliovalent substitution

By substituting lattice ions with ions of different valence, positively and negatively charged defects can be created as electron and hole traps with broad depth distribution that determines emission intensity and duration (Fig. 1b). For instance, the aliovalent substitution of Al^{3+} by Ge^{4+} and Mn^{4+} in a $LaAlO_3$ lattice resulted in persistent NIR luminescence that lasted for more than 20 hours[21]. Apart from acting as activators, high-valence Mn^{4+} ions can occupy octahedral sites of Al^{3+} ions and produce positively charged defects ($Mn_{Al}°$). Meanwhile, aliovalent substitution may create other types of defects, including positively charged $Al_I°$ interstitials (I, interstitial atom; °, positive charge) and $V_O°$ vacancies (V, vacancy; O, oxygen atom), as well as negatively charged V_{Al}' and V_{La}' vacancies (′, negative charge). In addition to generating electron/hole traps, aliovalent substitution can tune the local crystal field around the activators by varying the concentration of aliovalent dopants, resulting in trap redistribution and varied activator–trap interactions[22].

Non-stoichiometric synthesis

Non-stoichiometric compounds exhibit unique electrical or chemical properties due to the presence of particular defects; such compounds have found tremendous applications in solid-state electronic devices[23]. Such non-stoichiometry can be augmented by tuning the ionic stoichiometry of precursors (Fig. 1b), which has been shown to be effective in improving the optical performance of persistent luminescent phosphors[24]. For example, non-stoichiometric synthesis can generate Zn vacancies to trap holes in $Zn_{2.94}Ga_{1.96}Ge_2O_{10}:Cr^{3+}/Pr^{3+}$, which significantly increases the intensity and duration of NIR emission[25]. Similarly, non-stoichiometric synthesis can modulate the local crystal field by distorting the crystal lattice and modulating the coordination number of activators.

Lanthanide codoping

Lanthanide ions can be codoped into host materials to introduce extra, well-controlled trap states for the storage of charge carriers[26]. Using photoelectron spectroscopy data, the host-referred binding energy diagram can be established, providing the relative position of lanthanide's ground state with respect to the conduction band and valence band of the host material (Fig. 1c). Importantly, the shapes of double-zigzag lanthanide energy level curves can be easily reconstructed by referencing the host-referred binding energy value with Eu^{3+} (ref. [27]). YPO_4 is frequently used as a host material for lanthanide doping to generate persistent luminescence[28]. For divalent lanthanides with ground states within the host bandgap (such as Pr^{2+}, Nd^{2+}, Dy^{2+} and Tm^{2+}), their trivalent lanthanides can serve as electron acceptors. Notably, the large energy intervals between the conduction band and the ground state of Sm^{2+} and Yb^{2+} imply that doping with Sm^{3+} and Yb^{3+} leads to deep traps. In a similar way, host-referred binding energy diagrams have been used to analyse and predict persistent luminescence tuning for many lanthanide-codoped phosphors.

Selection of sintering atmosphere

For persistent luminescent phosphors prepared by high-temperature annealing, the sintering atmosphere can substantially affect their performance (Fig. 1d). Generally, a higher concentration of oxygen vacancies can be expected in a non-oxidizing atmosphere. These oxygen vacancies act as efficient electron traps below the conduction band minimum and provide persistent luminescence in many host materials[29]. For example, the persistent red luminescence of $Ca_2SnO_4:Gd^{3+}/Eu^{3+}$ phosphors sintered in a vacuum lasted much longer than those prepared in air. Moreover, persistent luminescence can be enhanced under a reducing atmosphere that favours the formation of oxygen vacancies in the host. Researchers found that $CaTiO_3:Cr^{3+}$ phosphors with NIR afterglow can be prepared only in a reducing atmosphere, indicating the crucial role of the annealing atmosphere in the synthesis of long-lived phosphors[30].

Temperature management

The kinetics of trap filling and release are inherently complex, mainly due to the simultaneous occurrence of filling and release processes. Compared to the charging process, shallow traps are much more likely to be depopulated. Therefore, charging at different temperatures can affect trap filling (Fig. 1e)[31]. At low temperatures above the thermal barrier for charging, traps can be filled at different depths because shallow traps are stable against weak thermal stimulation. As temperature increases, charge carriers in shallow traps become unstable, whereas deeply trapped charge carriers are only slightly perturbed. A further increase in temperature eliminates deep traps, reinvigorating luminescence intensity. For those phosphors in which shallow and intermediate traps are largely depleted after heating, diminished luminescence intensity and duration are observed when the temperature is lowered. By contrast, slightly increased luminescence can be obtained for phosphors that are charged at low temperatures with well-preserved shallow traps.

Pump power variation

During the charging process, trap filling and release coexist. When the excitation intensity varies, the thermoluminescence spectrum of

https://doi.org/10.1038/s41563-022-01468-y

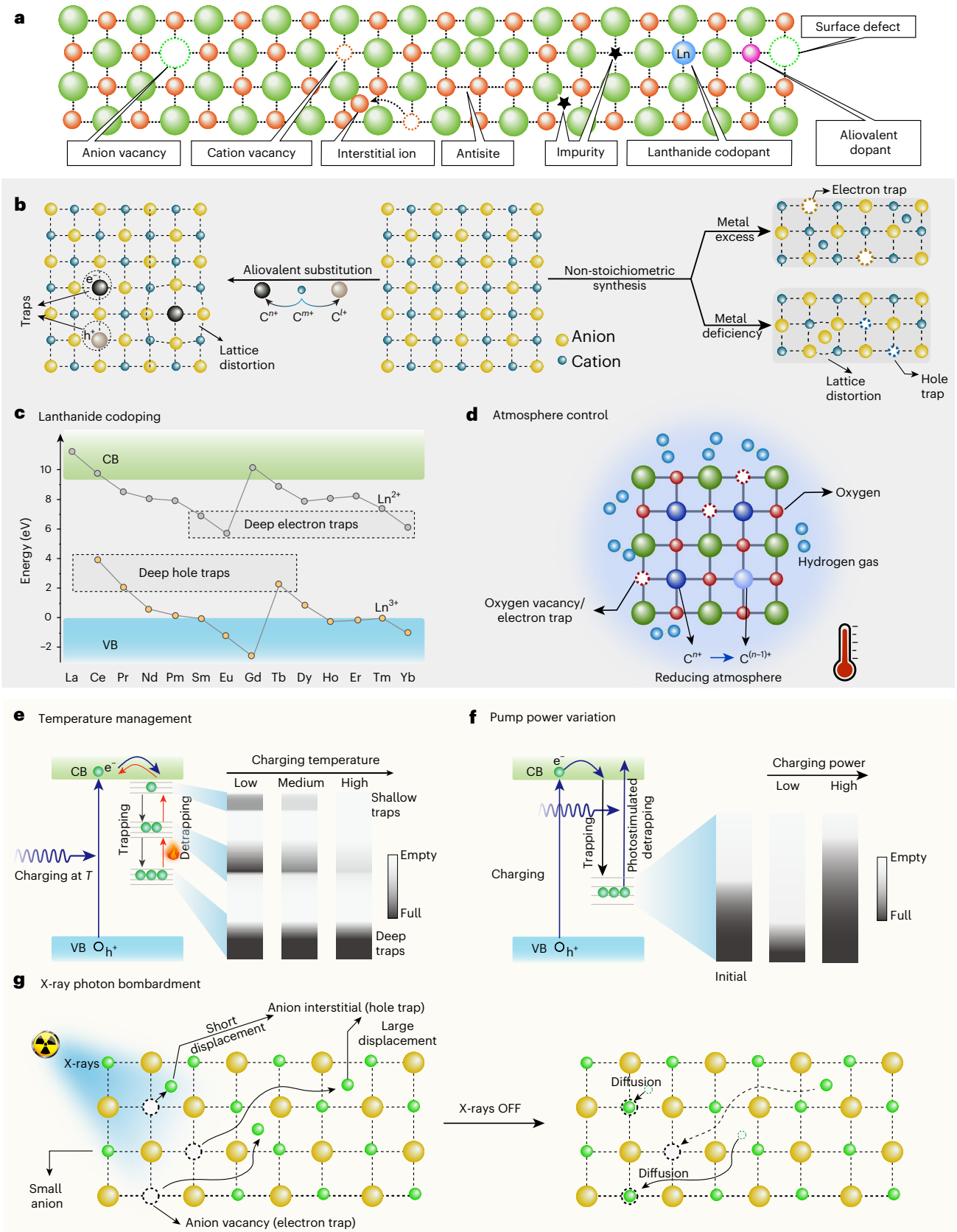

Fig. 1 | Common defects and strategies for trap manipulation in persistent luminescent materials. a, Possible point defects in inorganic host materials. Note that these defects may act as electron (e^-) or hole (h^+) traps to affect luminescence kinetics. **b**, Trap generation in crystal lattices by aliovalent substitution and non-stoichiometric synthesis. C, cation. **c**, Generation of charge carrier traps at targeted depths by codoping with lanthanide ions in YPO_4. CB, conduction band; VB, valence band. **d**, Luminescence modulation of persistent luminescent materials by annealing in different atmospheres. **e**,**f**, Control of trap filling by manipulation of charge temperature (T) and power density, respectively. **g**, X-ray irradiation can displace small anions and generate anion vacancies and interstitials that act as electron and hole traps, respectively. These displacements are reversible to some extent.

persistent luminescent phosphors does not vary appreciably, resulting in almost constant occupation of different traps. However, different excitation wavelengths produce significantly different trap filling and de-trapping capabilities for a certain phosphor, resulting in different trap occupancy situations[32]. For example, in the case of $LaMgGa_{11}O_{19}$:Cr^{3+} phosphors, upon 450 nm blue light-emitting diode (LED) charging, trapped charge carriers can partially escape from traps by absorbing the energy of the 450 nm photons, which leads to photon-induced trap depletion[33]. Therefore, low-power pumping at 450 nm cannot charge persistent phosphors because photon-induced de-trapping outperforms trapping (Fig. 1f). By contrast, the trapping rate can exceed the release rate when pumping at high power. This leads to charge carrier saturation and intense, long-lasting persistent luminescence.

X-ray photon bombardment

Bombardment with high-energy photons can displace small anions from their lattice to interstitial sites, creating anion Frenkel defects. Therefore, creating traps by high-energy photon irradiation instead of tuning synthesis parameters could be an efficient approach for trap manipulation. Recently, researchers found that X-rays can create electron and hole traps in lanthanide-doped fluorides, enabling highly efficient persistent luminescence in these nanosized phosphors (Fig. 1g)[6,34]. Experimental characterization and theoretical simulation show that fluoride anions are displaced to interstitial sites by high-momentum X-ray photons during elastic collisions. Importantly, the resulting fluoride vacancies and interstitials can act as electron/hole traps, triggering hours-long persistent luminescence from doped lanthanide activators. Notably, these displaced fluoride ions can diffuse back to their original sites, and this process can be facilitated by heating or light irradiation.

Luminescence spectral tuning

NIR-emitting phosphors can provide autofluorescence-free imaging in deep tissue with improved spatial resolution. To extend this toolkit and improve imaging depth and resolution, strategies such as activator selection, host variation and cascade energy transfer by codoping long-wavelength emitters can be applied to phosphor developments in the second (NIR-II, 1,000–1,350 nm) and even third (NIR-III, 1,500–1,800 nm) optical windows.

Activator selection

Transition metals, such as Mn^{2+}, Bi^{2+}, Ni^{2+} and Cr^{3+}, are commonly used as activators to generate persistent red/NIR luminescence with great flexibility in spectral tuning (Fig. 2a)[35–37]. For example, many Cr^{3+}-doped phosphors emit at 696 nm, especially with spinel $ZnGa_2O_4$ as the host[38,39]. Mn^{2+}-activated phosphors emitting in the spectral range of 560–820 nm have been developed in the photonic glass of calcium aluminium germanate[40]. In addition, Bi^{2+}-activated $SrSnO_3$ phosphors emit strongly at around 800 nm (ref. [41]). Remarkably, persistent luminescence can be extended into the 1,000–1,600 nm range when host materials are activated with Ni^{2+} (ref. [42]). Importantly, as a unique class of persistent luminescent emitters, trivalent lanthanide activators can cover almost the entire deep-UV–vis–NIR region. Recently, $NaYF_4$ nanocrystals with Er^{3+}, Ho^{3+}, Nd^{3+} or Tm^{3+} activators have been developed as efficient persistent luminescent NIR nanophosphors that enable long-term bioimaging and tracking with extremely high signal-to-noise ratios when charged with X-rays[6].

Host variation

For Ln^{3+} activators with 4*f* electrons shielded by 5*s* and 5*p* electrons, their luminescence mediated by the 4*f*–4*f* transition is insensitive to variations in the crystal field[43]. However, luminescence stemming from $4f^n$–$4f^{n-1}5d^1$ transitions is more sensitive to variations in the crystal field and could exhibit a large spectral shift when the host is changed. A representative example is the change of the host from $Sr_2MgSi_2O_7$ to $SrAl_2O_4$, which results in a large redshift of the Eu^{2+} luminescence from blue to green[44]. Since all *d* electrons are exposed to the lattice environment, transition metal activators mediated by *d*–*d* transitions are sensitive to the surrounding crystal field. For instance, the persistent luminescence spectrum of $ZnGa_2O_4$:Cr^{3+} shows a typical Cr^{3+} emission peak at 696 nm ($^2E \rightarrow {}^4A_2$)[4], whereas in an inverse spinel host, Zn_2SnO_4:Cr^{3+}, a broadband emission from 800 nm to 1,200 nm ($^4T_2 \rightarrow {}^4A_2$) dominates. What's more, Ni^{2+} with a 3*d* electron configuration (ref. [8]) is an excellent activator, glowing in the NIR-II and even NIR-III windows. For example, the stepwise substitution of Ga by Zn and Sn in $Zn_{1+y}Sn_yGa_{2-x-2y}O_4$:$Ni^{2+}$ can shift the broadband NIR luminescence from 1,300 nm to 1,500 nm (ref. [42]).

Cascade energy transfer

By coupling donor and acceptor activators, the energy of donor activators can be efficiently transferred to adjacent acceptor activators, enabling persistent NIR luminescence (Fig. 2c)[45]. Taking advantage of the broadband persistent luminescence of activators and the multiband absorption of lanthanide ions, most Ln^{3+} activators can be coupled to generate persistent NIR luminescence. Ce^{3+} and Cr^{3+} are frequently used as donors for coupling with Yb^{3+}, Nd^{3+} and Er^{3+} activators[46,47]. Efficient energy transfer from Ce^{3+} and Cr^{3+} to Ln^{3+} activators leads to persistent luminescence in the NIR-II and NIR-III ranges. To further enhance the persistent NIR luminescence, Ce^{3+} and Cr^{3+} donors are usually codoped with Ln^{3+} activators to form tri-activated systems[48]. The energy-transfer-mediated strategy for developing persistent luminescent NIR phosphors is quite robust and will contribute substantially to biological applications, especially if energy donors can be activated with deep-red or even NIR light.

Spectral multiplexing

Conventional persistent luminescent phosphors typically exhibit emission from only one type of doped activator. Recently, alkaline rare-earth fluoride nanocrystals were found to be efficient persistent luminescent nanophosphors upon X-ray irradiation[6,32]. Benefiting from their high feasibility in epitaxial multishell growth, multiple lanthanide activators can be integrated into a single nanoparticle with a core–multishell configuration (Fig. 2d). Since different activators can be well isolated in different layers, cross-relaxation between them can be largely minimized, leading to strong persistent luminescence from multiple activators simultaneously. Importantly, both the codopant combination and the doping concentration can be customized, which greatly enriches the multiplexing capability of these core–multishell nanophosphors. For example, by doping Nd^{3+}, Ho^{3+} and Er^{3+} separately in different spatial regions, a spectrally multiplexed nanophosphor can be prepared to exhibit intense NIR afterglow from all activators[6].

Luminescence enhancement

Persistent luminescent phosphors, especially at the nanoscale, usually feature low emission intensity due to severe surface quenching and a limited number of emitters. Consequently, an exposure duration of several seconds is usually required to capture images in a completely dark environment. Apart from the usual post-annealing treatment, surface passivation has also proven effective in minimizing surface quenching. Recently, organic dyes have been adopted as antennas to boost the light collection capacity of persistent luminescent phosphors. Moreover, enhancement of the local electromagnetic field through surface plasmon resonance can also enhance persistent luminescence.

Post-annealing

Although some phosphors exhibit persistent luminescence without post-annealing, most phosphors show no afterglow when the post-annealing step is omitted (Fig. 3a). Despite significant enhancement, post-annealing often leads to agglomeration. This agglomeration

https://doi.org/10.1038/s41563-022-01468-y

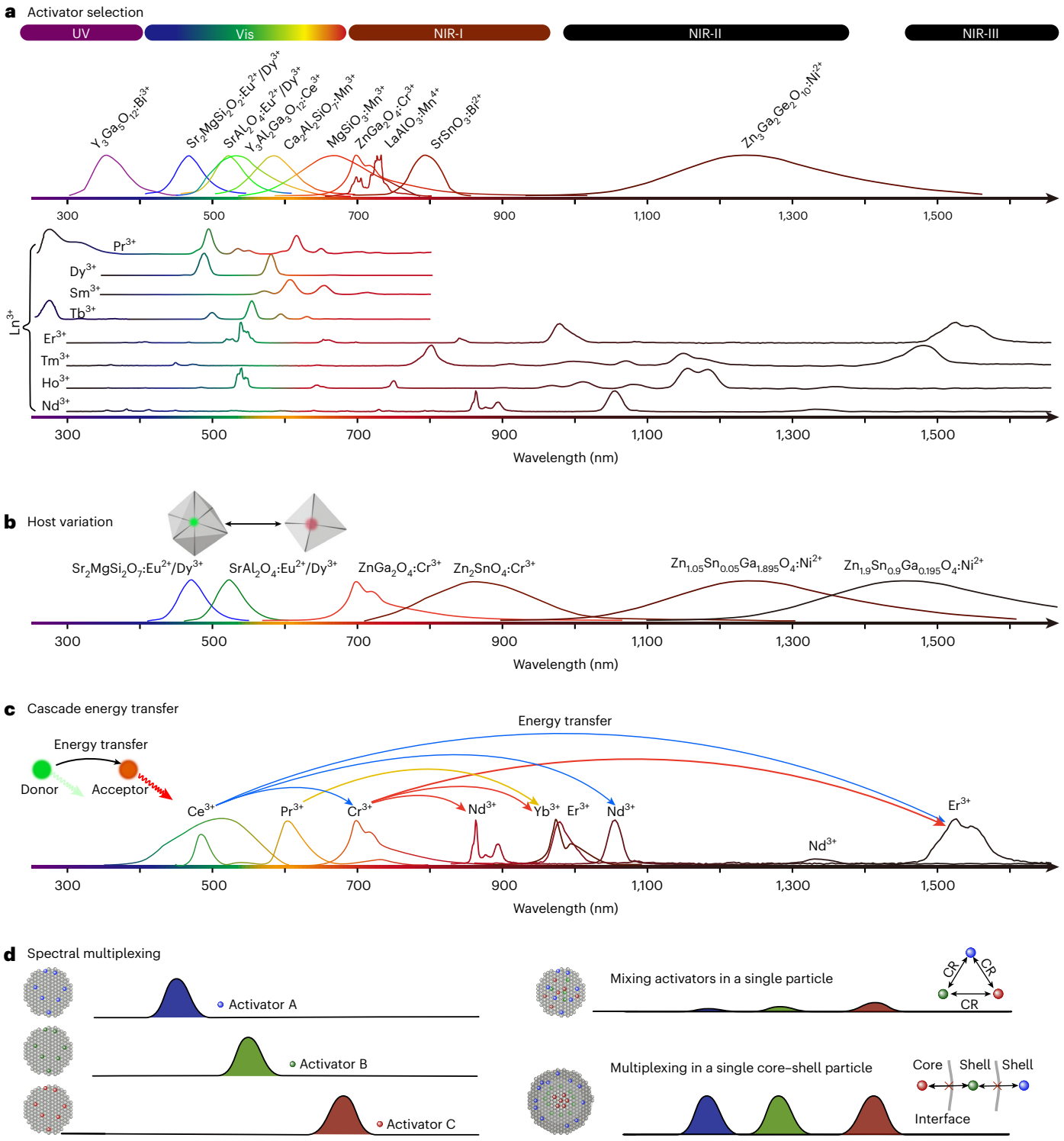

Fig. 2 | General strategies for tuning persistent luminescence in the UV, visible and NIR regions. a, Activator screening is efficacious in modulating persistent luminescence from the UV to the NIR region. **b**, Variation in host materials can tune the surrounding crystal field and exert control over luminescence profiles. The inset illustrates that a change in crystal field can affect the emission spectrum. **c**, Emission wavelength can be expanded by cascade energy transfer (inset schematic) between lanthanide activators. **d**, Doping different activators in a core–multishell nanoparticle can achieve persistent luminescent multiplexing at the single-particle level. CR, cross-relaxation.

has long been considered the major challenge in the development of bright nanophosphors. Recently, molten salt post-annealing was developed to synthesize monodisperse and bright persistent luminescent $ZnGa_2O_4:Cr^{3+}$ nanophosphors with minimal agglomeration[49]. Mixing persistent luminescent nanomaterials with molten salts ($NaNO_3$ and KNO_3) ensured good spatial isolation between adjacent nanomaterials during annealing, resulting in significantly enhanced luminescence with well-preserved morphology. Similarly, a SiO_2 surface coating was developed as an alternative to achieve spatial separation and reduce agglomeration[50].

https://doi.org/10.1038/s41563-022-01468-y

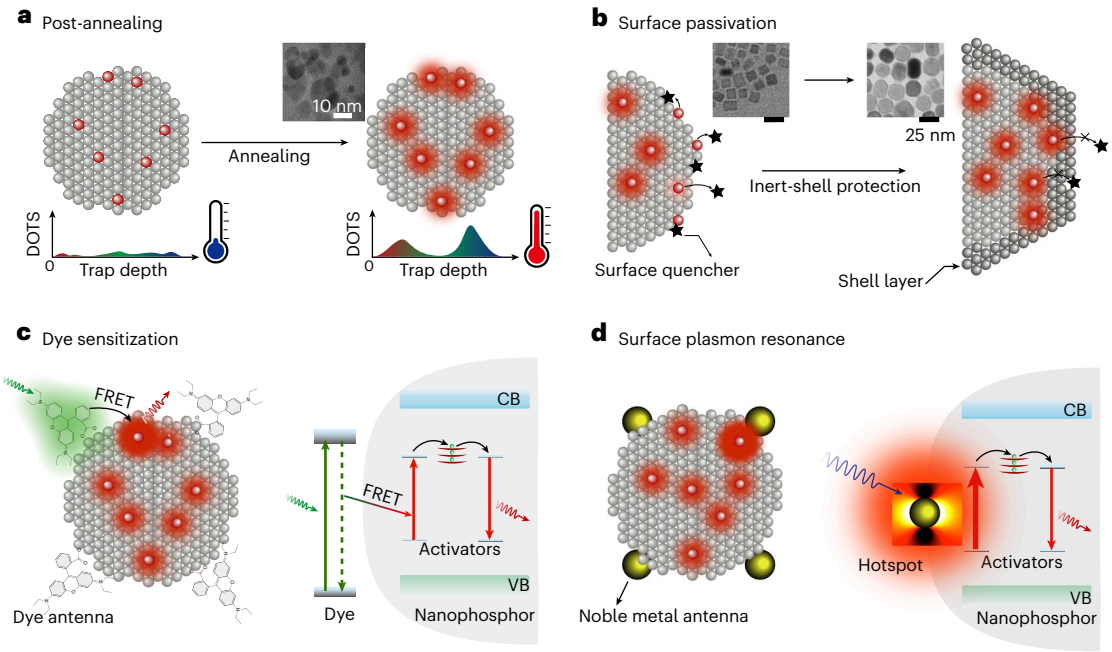

Fig. 3 | Common strategies to improve persistent luminescence of nanophosphors. a, Post-annealing increases the density of trap states (DOTS). Inset, transmission electron microscopy image of $ZnGa_2O_4$:Cr^{3+} nanoparticles after molten-salt-assisted annealing. **b**, Inert shell passivation minimizes the loss of luminescence induced by surface quenching. Inset: transmission electron microscopy images of CaF_2:Dy^{3+} core and CaF_2:Dy^{3+}@$NaYF_4$ core–shell nanoparticles. **c**, Dye sensitization boosts light collection through Förster resonance energy transfer (FRET). **d**, Surface plasmon resonance creates electric hotspots with high field intensity. Panels reproduced with permission from: **a**, ref. [49], Wiley; **b**, ref. [5], American Chemical Society.

Surface passivation

Since a large portion of emitters is exposed at the surface, nanophosphors suffer from surface quenching and exhibit lower brightness than their bulk counterparts. Surface passivation of $Zn_{1.2}Ga_{1.6}Ge_{0.2}O$:$Cr^{3+}$ nanophosphors with $Zn_{1.2}Ga_{1.6}Ge_{0.2}O$ or SiO_2 can effectively enhance the brightness and duration of persistent luminescence (Fig. 3b)[51]. In addition, growing a $NaYF_4$ layer on the surface of CaF_2:Dy nanoparticles can largely boost persistent luminescence[5]. This enhancement can be further improved by increasing the thickness of the passivation layer. Moreover, surface passivation with a SiO_2 layer is convenient for most persistent luminescent nanophosphors. However, the high phonon energy of the Si–O bond may act as an additional quenching source, resulting in limited performance enhancement.

Dye sensitization

Dye sensitization has been demonstrated to enhance the luminescence of lanthanide-doped up-conversion nanocrystals[52]. Because of the large absorption cross-sections (~10^{-16} cm^2) of organic dyes, dye sensitization can significantly enhance the light-harvesting capacity. For example, 5-carboxytetramethylrhodamine can be used as an organic antenna and modified on the surface of $ZnGa_2O_4$:Cr^{3+} nanomaterials[53]. Due to the spectral overlap between the emission of 5-carboxytetramethylrhodamine and the absorption of Cr^{3+} activators, the excitation energy absorbed by the antenna can be transferred to Cr^{3+} ions (Fig. 3c). Despite the enhanced persistent luminescence, dye sensitization to nanophosphors could introduce additional difficulties in surface modification for specific biological applications. Therefore, more effort should be devoted to molecular engineering when using this approach.

Surface plasmon resonance

Due to the intense light absorption and scattering of noble metal nanoparticles, surface plasmon coupling has been widely used for optoelectronic control[54]. As a result of the confinement of surface plasmons in nanoparticles, resonance peaks can be fine tuned from the visible to the NIR range by controlling the morphology, chemical composition and geometric structure of the nanoparticles (Fig. 3d). Surface plasmons can contribute to luminescence enhancement in two ways: (1) enhancing the light absorption of the host lattice and activators and (2) facilitating the radiative decay of the activators. To enhance persistent luminescence, the first strategy is usually used because the overlap between the resonance band and the absorption region of the phosphor benefits light harvesting and subsequent charge carrier generation. For example, the persistent luminescence of $Sr_2MgSi_2O_7$:Eu^{2+}/Dy^{3+} phosphors can be augmented up to an order of magnitude by surface deposition of sub-5 nm Ag or Cu nanoparticles[55,56].

Synthesis of persistent luminescent nanomaterials

Scientists have long considered post-annealing as a prerequisite for persistent luminescence, and almost all phosphors are habitually calcined, regardless of the synthesis method. However, this notion was revised in 2015 when ultrasmall $ZnGa_2O_4$:Cr^{3+} nanoparticles (~6 nm) exhibited intense, deep-red, persistent luminescence without post-annealing[57]. Annealing-free nanophosphors offer great flexibility in surface functionalization and great utility for biological applications. Although a long afterglow can be observed in these materials without calcination, calcination treatment can further improve their performance. In recent years, some new approaches for the synthesis of persistent luminescent nanomaterials have been developed (Table 1).

Template method

Mesoporous silica nanospheres (MSNs) are widely used for preparing uniform luminescent nanomaterials. For example, monodisperse SiO_2@$SrMgSi_2O_6$:Eu^{2+}/Dy^{3+} nanophosphors with a well-preserved morphology were prepared using MSNs (from 50–500 nm) as templates[58]. Similar approaches have also been used for the synthesis of various nanophosphors, such as SiO_2@$ZnGa_2O_4$:Cr^{3+} and SiO_2@$Gd_3Ga_5O_{12}$:

Table 1 | Synthetic tactics for persistent luminescent nanomaterials

Synthetic strategy	Host:dopants	Excitation source	Emission (nm)	Post-treatment	Morphology	Refs.
Sol–gel processing	$Ca_{0.2}Zn_{0.9}Mg_{0.9}Si_2O_6$: $Eu^{2+}/Dy^{3+}/Mn^{2+}$	X-rays/UV	690	1,050 °C for 10 h; wet grinding	Nanoparticle (50–100 nm)	85
	$Zn_{2.94}Ga_{1.96}Ge_2O_{10}$: Cr^{3+}/Pr^{3+}	UV	695	1,000 °C for 3 h; wet grinding	Nanoparticle (~50 nm)	25
	$ZnGa_2O_4$:Cr^{3+}	UV	695	Microwave-assisted combustion; grinding	Nanoparticle (6 nm)	86
Solvothermal/hydrothermal treatment	$ZnGa_2O_4$:Cr^{3+}	UV	695	750 °C for 5 h	Nanoparticle (40–100 nm)	67
	$ZnGa_2O_4$:Cr^{3+}	UV	696	Post-annealing free	Monodisperse nanoparticle (~9 nm)	4
	$ZnGa_2O_4$:Cr^{3+}	UV	695	Post-annealing free	Monodisperse nanoparticle (~7 nm)	73
Template method	$SrMgSi_2O_6$: Eu^{2+}/Dy^{3+}	UV	467	900 °C for 3 h	Tunable and uniform nanoparticle (50–500 nm)	58
	$ZnGa_2O_4$:Cr^{3+}	UV	696	600 °C for 2 h	Uniform nanoparticle (~150 nm)	59
	$ZnGa_2O_4$:Cr^{3+}/Sn^{4+}	UV	695	1,000 °C for 4 h	Spherical nanoparticle (~90 nm)	87
	$ZnGa_2O_4$:Cr^{3+}	UV	696	800 °C for 2 h	Carbon sphere template, hollow nanoparticle (~50 nm)	88
Coprecipitation/thermal decomposition	$NaLuF_4$:Tb^{3+}@$NaYF_4$	X-rays	492, 547	Post-annealing free	Uniform nanoparticle (~25 nm)	32
	$NaYF_4$:Er^{3+}@$NaYF_4$	X-rays	1000-1700	Post-annealing free	Tuneable and uniform nanoparticle (20–100 nm)	6
	CaF_2:Dy^{3+}@$NaYF_4$	X-rays/UV	480, 575	Post-annealing free	Uniform nanoparticle (20–50 nm)	5
Spatially isolated post-annealing	$ZnGa_2O_4$:Cr^{3+}	UV	695	Molten salt-assisted post-annealing at 650 °C for 6 h	Uniform nanoparticle (5–15 nm)	49
	$ZnGa_2O_4$:Cr^{3+}@SiO_2	UV	695	SiO_2 shell-assisted post-annealing at 850 °C for 3 h	50–100 nm SiO_2 spheres containing multiple ~10 nm $ZnGa_2O_4$:Cr^{3+} nanoparticles	50
Laser ablation	$Ca_2Si_5N_8$:Eu^{2+}/Tm^{3+}	UV	610	Post-treatment free	Nanoparticle (~5 nm)	65
	$ZnGa_2O_4$:Cr^{3+}	UV	695	Post-treatment free	Nanoparticle (2–5 nm)	64

Cr^{3+}/Nd^{3+} (ref. [59]). Importantly, the template method enables the functionalization of drugs and photosensitizers for diagnostics and therapeutics in nanomedicine. Although size-tunable, monodisperse nanophosphors can be obtained using the template method, the overall size of the phosphors is determined by the chosen template, which is usually larger than 100 nm and is not ideal for biological applications. In addition, the nanochannels in silica nanospheres are typically annealed at low temperatures to prevent collapse, resulting in limited enhancement of luminescence. Surfactant-assisted self-assembly has been developed as an advanced bottom-up strategy to construct mesoporous metal oxide nanostructures, including TiO_2 and Al_2O_3 (ref. [60]). Considering their high mechanical stability at high temperatures, we believe that these mesoporous metal oxides can serve as next-generation nano-templates.

Coprecipitation and thermal decomposition

Coprecipitation and thermal decomposition are common approaches for synthesizing metal oxide and fluoride nanoparticles[61]. Researchers have found that lanthanide-doped fluoride nanoparticles synthesized by these methods can emit intense persistent luminescence after X-ray excitation[62]. By using a non-coordinating high-boiling-point solvent (1-octadecene) as the primary solvent and oleic acid as a passivating ligand to prevent agglomeration, precursors such as lanthanide acetate and trifluoroacetate are precipitated or decomposed at high temperature (~300 °C) to form highly monodisperse nanocrystals. The size of the nanoparticles can be tuned from sub-10 to 100 nm by controlling parameters such as temperature, reaction time and host composition. The emission band from the UV to the NIR region can be well controlled by selecting different lanthanide dopants[34,63]. Importantly, core–shell structures can be easily prepared by epitaxial growth to enable multicolour emissions at the single-particle level[5,6].

Pulsed laser ablation method

A pulsed laser can deliver a large amount of energy in a high concentration to the target in a liquid (for example, water, acetone, ethanol or ethyl acetate), creating a high impact pressure on target surfaces to produce nanoparticles with the same chemical composition as the bulk target. This low-cost top-down method to reduce bulk targets to the nanoscale has already been used to produce persistent luminescent nanoparticles[64]. For example, ablation of a $SrAl_2O_4$:Eu^{2+}/Dy^{3+} pellet

Table 2 | Details of representative persistent NIR luminescent nanomaterials

Host:dopants	Excitation source	Exposure time	Emission (nm)	Duration	Refs.
$ZnGa_2O_4:Cr^{3+}/Sn^{4+}$@MSNs	UV (6 W, 254 nm for 5 min)	60 s (subcutaneous injection, (2 mg ml^{-1}), 60 µl)	696	>2 h	89
SiO_2@$Zn_{0.6}Ca_{0.4}Ga_2O_4:Cr^{3+}/Yb^{3+}$	UV (6 W, 254 nm for 10 min)	1 s (chicken breast, 0–7 mm)	696, 980	>2 h	90
$NaYF_4$:Er@$NaYF_4$; $NaYF_4$:Nd@$NaYF_4$; $NaYF_4$:Ho@$NaYF_4$; $NaYF_4$:Tm@$NaYF_4$	X-rays (~200 Gy)	10 s (intravenous injection, 0.2 mM, 15 µl)	800, 980, 1,525 860, 1,064 1,180 1,190, 1,475	>72 h	6
$Zn_2Ga_3Ge_{0.75}O_8:Cr^{3+}/Nd^{3+}$	X-rays (0.55 Gy) Visible (635 nm, 5 min)	Not available (<2.5 cm pork tissue)	696, 1,067	>16 h	91
$Zn_2Ga_2Sn_{0.5}O_6:Yb^{3+}/Ni^{2+}$	UV (254 nm for 5 min)	Not available	1,350	5 min	92
$MgGeO_3:Mn^{2+}/Yb^{3+}/Li^+$	UV (6 W, 254 nm for 5 min)	60 s (intravenous injection, 10 µg ml^{-1})	680, 980	>7 h	93
$Y_3(Al/Ga)_5O_{12}:Ce^{3+}/Cr^{3+}/Nd^{3+}$	Visible (410 nm, 3 W for 10 min)	3 s (0–20 mm chicken breast)	508, 860, 1,064	>1 h	94
$LaGaO_3:Sb^{3+}/Cr^{3+}$	X-rays (0.37 Gy)	60 s (intravenous injection, 200 µl, 2 mg ml^{-1})	750	>500 h	95
$CaSnO_3:Bi^{3+}$	Visible (700 nm, 3 mW cm^{-2} for 30 min)	N.A.	810	>1 h	96
$GdAlO_3:Cr^{3+}/Sm^{3+}$	UV (254 nm for 5 min)	60 s (intravenous injection, 200 µl, 1 mg ml^{-1})	732	>0.5 h	97

target in acetone or ethanol with a 1,064 nm pulsed neodymium-doped yttrium–aluminum–garnet (Nd:YAG) laser at 10 Hz produced $SrAl_2O_4:Eu^{2+}/Dy^{3+}$ nanoparticles (~7.5 nm) with a narrow size distribution. Interestingly, the morphology of the produced nanophosphors can be controlled well by adjusting parameters such as pulse energy, laser wavelength, pulse frequency and pulse width. Moreover, persistent luminescent $ZnGa_2O_4:Cr^{3+}$ and $Ca_2Si_5N_8:Eu^{2+}/Tm^{3+}$ nanophosphors have also been prepared using this technique[64,65].

Biological applications

The great successes of the past decade in developing persistent NIR luminescent nanophosphors (Table 2) have opened new opportunities for traditional phosphors. Compared with organic dyes, quantum dots and lanthanide-doped up-conversion nanocrystals, imaging using persistent luminescent nanophosphors has enabled the complete elimination of biological autofluorescence and photodamage (Table 3). Moreover, the high photostability and flexibility in surface functionalization of these nanophosphors facilitate their rapid development in applications, especially in high-sensitivity biosensing, long-term monitoring of cell activity and theranostics.

Since persistent luminescent nanophosphors can store absorbed photoenergy, and because the luminescence intensity varies as a function of time after excitation is terminated, the definition of quantum yield for conventional luminescent materials does not apply to persistent luminescent phosphors. Upon UV excitation, an absolute quantum yield of ~10% has been reported for NIR-emitting persistent luminescent nanophosphors ($Zn_{1.25}Ga_{1.5}Ge_{0.25}O_4:Cr^{3+}/Yb^{3+}/Er^{3+}$)[66]. However, for an accurate assessment of the photon conversion capability of persistent luminescent materials, long-term time-resolved absorption (or reflection) and emission spectra should be recorded using an integrating sphere.

Although slightly inferior to organic persistent luminescent materials in terms of biocompatibility and luminous intensity, nanocrystalline persistent luminescent materials have great advantages in the following aspects.

(1) Crystalline nanophosphors have much higher photostability, and photobleaching could be eliminated.
(2) Emission wavelength can be tuned to the NIR-II and NIR-III ranges by rational doping.
(3) The performance of these nanophosphors is not affected by the surrounding biochemical environment, such as oxygen content.
(4) Mixing and encapsulation of multiple components are not required, which enables ultrasmall physical dimensions (smaller than 10 nm).
(5) Crystalline nanophosphors can be activated by X-rays for deep-tissue imaging.

Autofluorescence-free biosensing

Using NIR as the excitation source, lanthanide-doped up-conversion nanocrystals have been extensively employed for background-free biosensing. However, due to their low conversion efficiency, high-power laser illumination is required. Time-gated luminescence detection has proven effective in increasing sensitivity by blocking short-lived autofluorescence. However, this technique complicates instrumentation. Because luminescence persists for hours, the time-gated technique can be applied to long-lived luminescent nanophosphors that avoid time-resolved spectroscopy[8]. As illustrated in Fig. 4a, a strong autofluorescence of the mouse would significantly mask the fluorescence signal from nanophosphors. The imaging contrast over an emitting region with persistent luminescent nanophosphors can be greatly enhanced if the autofluorescence is removed after excitation ceases. For example, by comparing the in vivo imaging of $ZnGa_2O_4$:Cr and commercial quantum dots with similar emission spectra (emitting at 705 nm) in living mice, researchers found that the signal-to-noise ratio is highly in favour of persistent luminescent nanomaterials, with a signal-to-noise ratio increasing from ~17 for quantum dots to 186 for $ZnGa_2O_4$:Cr nanoparticles following intramuscular injection[67]. What's more, the signal-to-noise ratio can be improved to ~1,000 when X-ray-activated NIR-emitting $NaYF_4$:Nd nanoparticles (1,064 nm emission) are used for imaging[6].

In 2011, a persistent luminescent nanomaterial was reported to mediate autofluorescence-free biosensing using a luminescence turn-on approach. Through electrostatic interaction, conjugates of α-fetoprotein antibody and gold nanoparticles were bound to the surfaces of polyethyleneimine-functionalized $Ca_{1.86}Mg_{0.14}ZnSi_2O_7:Eu^{2+}/Dy^{3+}$ nanophosphors, and the persistent luminescence of the latter could be quenched by the former through efficient energy transfer. The presence of α-fetoprotein resulted in the desorption of gold

Table 3 | Main features of luminescent nanomaterials for bioapplications

Nanophosphors	Size (nm)	Photochemical stability	Toxicity	Excitation	Emission	Lifetime	Absolute quantum yield	Bioconjugation	SNR	Refs.
Organic dyes	<1	Low (insufficient for high-light flux applications)	Low to high	UV–Vis–NIR	Vis–NIR-II	1–10 ns	50–100%	Easy (the best choice for fine structure labelling)	Low (<50)	98
Fluorescent proteins	~5	Low (higher than organic dyes)	No	UV–Vis	Vis–NIR (<900 nm)	1–100 ns	10–80%	Easy	Low (<50)	99,100
Aggregation-induced emission luminogens	<10	Fair	Low	UV–Vis	Vis–NIR-II	1–20 ns	<90%	Easy	Low (<50)	101–103
Room-temperature Phosphorescence nanomaterials	Sub-10 to larger than 100	Fair	Low	UV–Vis	Vis–NIR (<900 nm)	Tens to thousands of milliseconds	<50%	Easy	High (>400, large redshift)	13,104
Organic long persistent luminescence systems	10–100	Fair	Low	UV–Vis	Vis–NIR (<900 nm)	Tens of minutes	1–50% upon excitation in N_2	Need encapsulation. Suitable for tissue-level imaging.	Ultrahigh (even higher than 1,000)	14–16
Carbon dots	<10	High and blinking	Low	UV–Vis	Vis–NIR (<750 nm)	Nanoseconds to milliseconds	Sub-10% to 80%	Moderate easy (easy for surface modification)	Low (<10)	105,106
Quantum dots	2–10	High and blinking	High (heavy metal leakage can be reduced with coating)	UV–Vis-NIR	UV–Vis–NIR-III	10–100 ns (nulti-exponential decay)	Sub-10% to near unity (strong absorption)	Moderate easy (easy for surface modification)	Moderate (<50)	106,107
Fluorescent nanodiamonds	2–20	Ultrahigh	Low (biocompatible coating is possible)	UV–Vis	Vis–NIR (500–850 nm)	~25 ns	70–80%	Moderate easy (easy for surface modification)	High (microwave modulation-assisted imaging)	108,109
Upconversion nanoparticles	10–50	Ultrahigh	Low (biocompatible coating is possible)	NIR	UV–Vis–NIR-II	Sub-10 μs to tens of milliseconds	<10% (power dependent)	Moderate easy (high flexibility in surface modification)	High (~100, depth-dependent)	110
Inorganic persistent luminescent nanomaterial	5–100	Ultrahigh	Low (can be well coated)	X-rays–UV–Vis–NIR (Suitable for deep-tissue imaging)	UV–Vis–NIR-III	Up to tens of hours	Hard to define (<25% upon excitation)	Moderate easy (high flexibility in surface modification)	Ultrahigh (up to 1,000, depth-dependent)	6,66,111

nanoparticles and triggered persistent luminescence, and a detection limit of 410 ng l^{-1} was measured[68]. What's more, microbial metabolism can also be monitored using persistent luminescent nanoprobes. Recently, persistent luminescent Zn_2GeO_4:Mn@Fe^{3+} nanoprobes have been designed for real-time and dynamic monitoring of Fe(III) respiration metabolism[69]. Since Fe^{3+} can be reduced to Fe^{2+} by electrons transmitted across the cell membrane of microorganisms during Fe(III) respiration, the Fe^{3+}-induced persistent luminescence quenching of Zn_2GeO_4:Mn@Fe^{3+} can be gradually relieved, and the ratio of Fe^{2+} to Fe^{3+} can be indicated by the luminescence intensity.

Despite the improved detection sensitivity, the continuous decay of persistent luminescence during data acquisition usually leads to unavoidable measurement errors. Because signal fluctuations caused by instrument performance and changes in the external environment can be effectively eliminated by self-calibration of the internal reference signal, ratiometric fluorescence sensing has attracted considerable interest to further improve biosensor performance (Fig. 4b). By coupling persistent luminescent nanomaterials with rhodamine B, the detection limit of ratiometric biosensing for prostate-specific antigen, for example, can reach 90 ng l^{-1} (ref. [70]). Although this value is still below the commercially available immunoassay (<50 ng l^{-1})[71], much brighter persistent luminescent nanomaterials could improve performance significantly. Importantly, minimizing the light dose enables the biosensing of photosensitive analytes using persistent luminescent nanomaterials with high accuracy.

Long-term, real-time, deep-tissue imaging

Persistent NIR luminescence can be recorded continuously for several minutes after excitation ceases, and luminescence can be recovered repeatedly upon NIR stimulation, allowing long-term data acquisition. However, when electrons in deep traps are exhausted, NIR stimulation no longer works. Therefore, to completely remove the time limitation for imaging, nanophosphors that allow on-site charging over multiple cycles should be developed (Fig. 4c). To this end, lanthanide ions such as Yb^{3+}/Er^{3+} were integrated into nanophosphors to trigger persistent luminescence for bioimaging upon NIR excitation (150 mW cm^{-2} at 980 nm); however, the luminescence intensity was limited by the low up-conversion efficiency (<1%)[72]. For Cr^{3+}-activated nanophosphors that benefit from the broad excitation band from 350 to 650 nm, these phosphors can be recharged with white LEDs[60,73,74], and multi-cycle imaging at a tissue depth of ~10 mm has been demonstrated. Compared to visible or NIR light, X-rays have a higher photon energy

https://doi.org/10.1038/s41563-022-01468-y

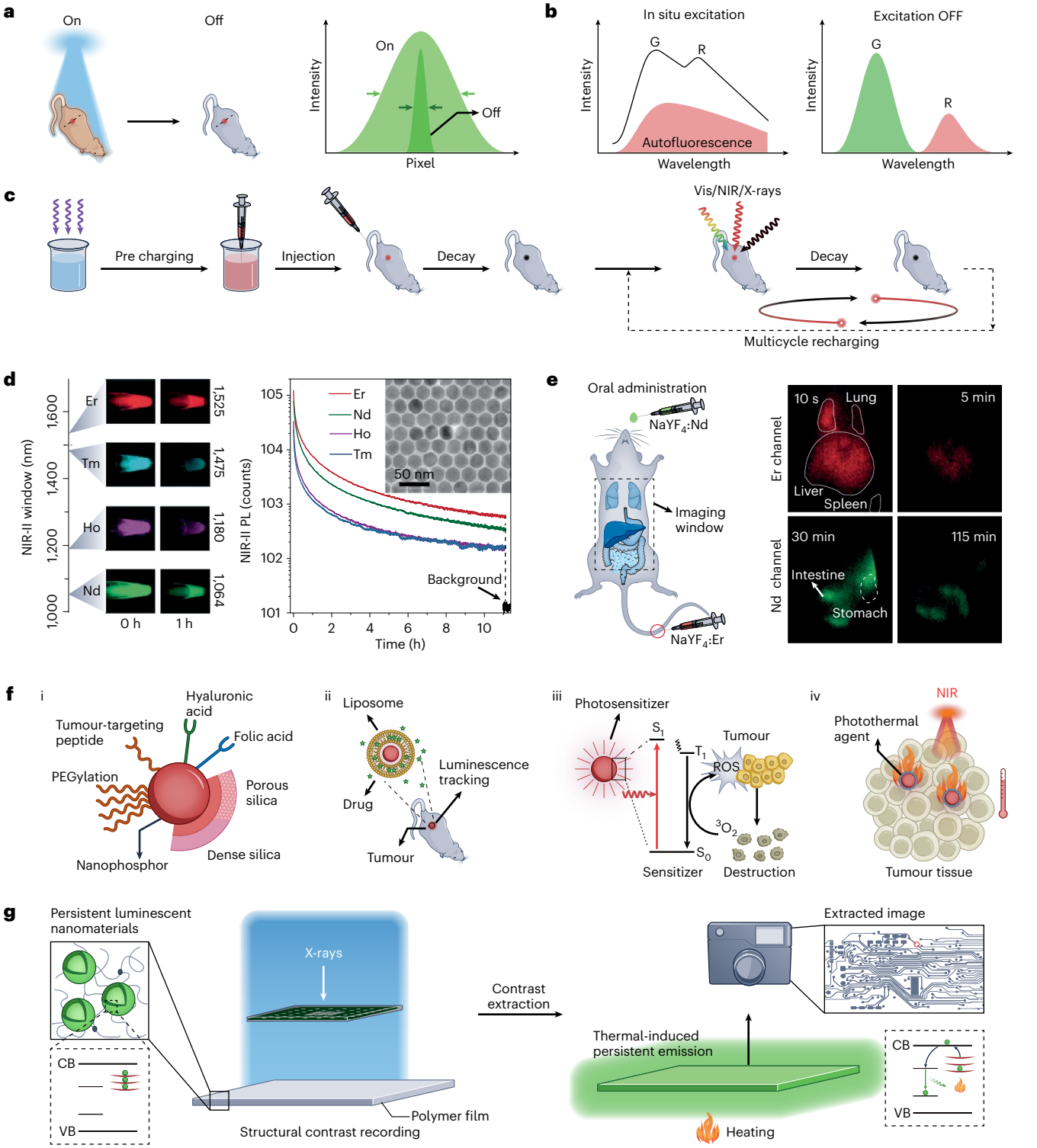

Fig. 4 | Persistent luminescent nanomaterials for autofluorescence-free biological applications. a, Demonstration of high-resolution imaging. The right panel illustrates the variation of full-width at half-maximum of a persistent luminescent region before and after excitation. **b**, Illustration of the principle of ratiometric fluorescence biosensing using persistent luminescent nanophosphors. G, green. R, red. **c**, Deep-tissue imaging process using persistent luminescent nanomaterials that can be recharged by visible, NIR or X-ray irradiation. **d**, NIR-II persistent photoluminescence (PL) images of Nd-, Ho-, Tm- and Er-activated nanoparticles in centrifuge tubes, and luminescence decay curves of typical emission bands. Inset: transmission electron microscopy image of the as-prepared nanoparticles. **e**, Real-time tracking of the biodistribution of persistent luminescent nanomaterials in different organs. The schematic on the left shows the set-up. **f**, Surface functionalization approaches for enhanced biocompatibility and targeting efficiency (i). Principles of persistent-luminescent-nanomaterial-mediated theranostics for autofluorescence-free bioimaging-guided chemotherapy (i and ii), photodynamic therapy (iii) and photothermal therapy (iv). ROS, reactive oxygen species. **g**, Persistent luminescent nanomaterials for high-resolution X-ray imaging. Panels **d** and **e** adapted with permission from ref. [6], Springer Nature Limited.

and much lower attenuation efficiency in living tissue. For example, $ZnGa_2O_4:Cr^{3+}$ nanophosphors could be imaged underneath 20 mm of deep tissue for multicycle imaging after charging with X-rays (45 kV, 0.5 mA, 5 min)[63]. Recently, it was demonstrated that lanthanide-doped $NaLnF_4$ nanocrystals containing activators such as Er^{3+}, Tm^{3+}, Ho^{3+} and Nd^{3+} can emit persistent luminescence in the NIR-I and NIR-II regions after X-ray irradiation (Fig. 4d)[6]. By oral administration and intravenous injection of these NIR-emitting nanophosphors, systemic circulation of nanophosphors in multiple organs can be unambiguously recorded over hours with a high signal-to-noise ratio (Fig. 4e).

Theranostics

Integration of deep-tissue autofluorescence-free bioimaging with emerging therapeutic techniques offers great opportunities for in vivo disease diagnosis and therapeutic efficacy monitoring. Rational surface functionalization confers nanophosphors with high stability in biological media, low cytotoxicity and improved targeting (Fig. 4f(i))[75]. For instance, polyethylene glycol and silica coatings can significantly enhance the systematic distribution of nanophosphors[74]. Moreover, tumour-targeting agents, such as peptides and folic acid, can be conjugated with phosphors to enhance their targeting. Flexibility in surface functionalization allows the development of persistent luminescent nanophosphors for drug loading and image-guided chemotherapy (Fig. 4f(ii)). For example, coating NIR-emitting nanophosphors with liposomes enables the encapsulation of antitumour drugs such as paclitaxel. After intravenous injection, these drug-loaded nanocomposites can accumulate in the tumour and enable effective cancer therapy[76]. Importantly, upon LED charging, the evolution of the nanocomposite distribution, especially at the tumour site, can be monitored continuously without autofluorescence for more than 24 hours.

Apart from chemotherapeutic agents, photosensitizers could also be coupled with nanophosphors to construct nanoplatforms for photodynamic therapy[62,77]. Through non-radiative energy transfer or reabsorption, photosensitizers integrated into the nanoplatform can be activated by absorbing energy from adjacent nanophosphors (Fig. 4f(iii)). Cytotoxic radicals and reactive oxygen species (ROSs) are then generated incessantly to kill cancer cells[78]. In photodynamic therapy with deep-red or NIR rechargeable nanophosphors, therapeutic efficacy can be significantly improved in deep tissue by repeated charging. However, although the use of persistent luminescent nanophosphors can avoid overheating and tissue damage from long-term in situ irradiation, the formation of cytotoxic radicals and ROSs is reduced due to the much lower photon flux.

As an extension of photodynamic therapy, photosensitizers with a high NIR-photon-to-heat conversion efficiency can be integrated with persistent luminescent nanophosphors to construct nanoplatforms for photothermal therapy (Fig. 4f(iv)). When illuminated with NIR light, the incident photons can be efficiently used by photothermal agents and cause a local temperature increase to above 50 °C to kill cancer cells. By mapping persistent luminescence, the targeted delivery of nanophosphors and their distribution after therapy can be clearly determined.

X-ray imaging

Lanthanide-doped $NaLuF_4$ nanocrystals can emit luminescence for up to 30 days after irradiation with X-rays (50 kV, 1 mA, 10 min)[32]. Various lanthanide activators can be used to tune the colour of the persistent luminescence from blue to red. $NaLuF_4$:Tb(15 mol%)@$NaYF_4$ nanophosphors exhibit the brightest luminescence and disperse well in a polydimethylsiloxane substrate. Upon X-ray irradiation, the pattern containing the structural information of a particular object can be stored by these long-lived persistent nanophosphors. When heated, the rapid release of the trapped charge carriers produces persistent luminescence that allows imaging of highly curved electronic circuit boards with a digital camera (Fig. 4g). Moreover, the high flexibility of lanthanide-activated long-lived phosphors in colour tuning has found applications in multiplexed optical data storage[34]. Since lanthanide activators have fingerprint-like emission bands covering the deep-UV to NIR-II range, the storage capacity of these phosphors can be significantly extended by printing multiple layers, each with different activators[79].

Photochemical tissue bonding in clinical settings has recently emerged as a new application of persistent luminescent materials in addition to biosensing, imaging and theranostics[80]. Upon UV light charging, ZnS:Ag,Co particles were used as persistent light sources, and their green luminescence can be efficiently absorbed by the Rose Bengal molecules in conjugates of hyaluronate and Rose Bengal that are widely distributed in the collagen layer. Through interaction between activated Rose Bengal molecules and collagen, collagen-free radicals can be generated to initiate the formation of covalent bonding between collagen molecules and facilitate tissue bonding. Since persistent luminescent materials can work without in situ excitation, they are capable of photochemical tissue bonding in deep tissues (even at centimetre levels).

Future perspectives

Although we have succeeded in producing ultrasmall and uniform nanophosphors, significant challenges still lie ahead to harness the effects of persistent luminescence for technological applications. It is not essential for in vitro biosensing to use small persistent luminescent nanophosphors. However, in practical imaging applications, smaller particles (<10 nm) are often employed for more precise labelling of cellular structures. In addition, it is highly desirable to prepare persistent luminescent nanophosphors with a large number of traps to store excitation energy and achieve near-unity light yield with minimal non-radiative loss.

One of the current priorities is to expand the synthetic toolbox for persistent luminescent nanophosphors beyond $ZnGa_2O_4:Cr^{3+}$ phosphors and their derivatives. We also need to explore strategies to preserve nanophosphor morphology during annealing. In addition, we need to continue to search for new synthesis protocols that no longer require post-annealing.

Another challenge for bioimaging applications is the low persistent luminescence intensity, especially at the single-particle level. The photon flux of a single nanophosphor can quickly drop far below the detection limit after an excitation pulse, making real-time tracking in living cells challenging. Compared with shallow traps, deep traps have a much lower thermally stimulated release rate. Therefore, photon flux from deep traps was very limited for detection. Since those deep traps can be efficiently pumped to fill shallow traps upon NIR stimulation, a short but strong persistent luminescence from newly filled shallow traps can be sustained by intermittent light stimulation. A high density of shallow traps is necessary to accommodate charge carriers extracted from deep traps, and it is also critical to achieving a high density of deep traps to counteract the depletion caused by intermittent excitation. For this reason, it is quite important for the community to develop practical approaches for customizing the trap depth and density.

To complement experimental characterization techniques, quantum mechanical calculations such as density functional theory have proven useful for identifying and characterizing defects in a wide range of materials when combined with a thermodynamic formalism[81,82]. Calculable parameters, including the defect formation energy, the thermodynamic transition level and the position of defect levels with respect to the host conduction band minimum and valance band maximum, can provide additional perspectives for understanding the complex kinetics of charge carrier trapping and discharge processes. By employing existing computational and experimental data as input, emerging artificial intelligence techniques, such as machine learning, could be used to reveal the structure–property correlation, facilitating the optimization of existing persistent luminescent materials and the development of novel alternatives with improved optical performance[83].

Another long-standing problem is that all persistent luminescent nanophosphors feature inefficient charging with visible and NIR light. In addition to developing phosphors with narrow bandgaps, heterojunction materials may provide a solution to this problem. By sensitizing persistent luminescent nanophosphors with Vis–NIR sensitizers, such as quantum dots with large absorption cross-sections, efficient harvesting of deep-red and even NIR illumination is possible due to interfacial exciton charge transfer from surface-bound sensitizers to nanophosphors.

As with luminescent nanomaterials such as up-conversion nanoparticles and quantum dots, imaging applications with persistent luminescent nanomaterials are currently limited to small animals. Human imaging applications of persistent luminescent nanomaterials are limited to very shallow depths under the skin because of strong light attenuation. The ability to emit persistently after excitation makes these materials highly promising for theranostics or photoreactions in deep tissues where X-rays can be effective. However, because nanomaterials are frequently over 10 nm in size, they cannot be rapidly excreted through kidneys via urine, but rather must go through hepatobiliary clearance in an extremely inefficient manner[84]. Therefore, the ultimate goal of the community is to develop persistent luminescent nanomaterials characterized by an ultrasmall size (<5 nm) and a strong afterglow.

Online content

Any methods, additional references, Nature Portfolio reporting summaries, source data, extended data, supplementary information, acknowledgements, peer review information; details of author contributions and competing interests; and statements of data and code availability are available at https://doi.org/10.1038/s41563-022-01468-y.

References

1. Lastusaari, M. et al. The Bologna Stone: history's first persistent luminescent material. *Eur. J. Mineral.* **24**, 885–890 (2012).
2. Hölsä, J. Persistent luminescence beats the afterglow: 400 years of persistent luminescence. *Electrochem. Soc. Interface* **18**, 42–45 (2009).
3. Shionoya, S., Yen, W. M. & Yamamoto, H. *Phosphor Handbook* (CRC Press, 2018).
4. Li, Z. et al. Direct aqueous-phase synthesis of sub-10 nm "luminous pearls" with enhanced in vivo renewable near-infrared persistent luminescence. *J. Am. Chem. Soc.* **137**, 5304–5307 (2015).
5. Huang, K. et al. Three-dimensional colloidal controlled growth of core–shell heterostructured persistent luminescence nanocrystals. *Nano Lett.* **21**, 4903–4910 (2021).
6. Pei, P. et al. X-ray-activated persistent luminescence nanomaterials for NIR-II imaging. *Nat. Nanotechnol.* **16**, 1011–1018 (2021).
7. Zhuang, Y., Wang, L., Lv, Y., Zhou, T.-L. & Xie, R.-J. Optical data storage and multicolor emission readout on flexible films using deep-trap persistent luminescence materials. *Adv. Funct. Mater.* **28**, 1705769 (2018).
8. Zhao, X. et al. Autofluorescence-free chemo/biosensing in complex matrixes based on persistent luminescence nanoparticles. *TrAC Trends Anal. Chem.* **118**, 65–72 (2019).
9. Lecuyer, T. et al. Chemically engineered persistent luminescence nanoprobes for bioimaging. *Theranostics* **6**, 2488–2524 (2016).
10. Huang, K. et al. Designing next generation of persistent luminescence: recent advances in uniform persistent luminescence nanoparticles. *Adv. Mater.* **34**, 2107962 (2021).
11. Becker, R. S. *Theory and Interpretation of Fluorescence and Phosphorescence* (Wiley-Interscience, 1969).
12. Lewis, G. N. & Kasha, M. Phosphorescence and the triplet state. *J. Am. Chem. Soc.* **66**, 2100–2116 (1944).
13. Zhao, W., He, Z. & Tang, B. Z. Room-temperature phosphorescence from organic aggregates. *Nat. Rev. Mater.* **5**, 869–885 (2020).
14. Kabe, R. & Adachi, C. Organic long persistent luminescence. *Nature* **550**, 384–387 (2017).
15. Jinnai, K., Kabe, R., Lin, Z. & Adachi, C. Organic long-persistent luminescence stimulated by visible light in p-type systems based on organic photoredox catalyst dopants. *Nat. Mater.* **21**, 338–344 (2022).
16. Jiang, Y. et al. A generic approach towards afterglow luminescent nanoparticles for ultrasensitive in vivo imaging. *Nat. Commun.* **10**, 2064 (2019).
17. Guo, Q., Liao, L., Mei, L., Liu, H. & Hai, Y. Color-tunable photoluminescence phosphors of Ce^{3+} and Tb^{3+} co-doped $Sr_2La_8(SiO_4)_6O_2$ for UV w-LEDs. *J. Solid State Chem.* **225**, 149–154 (2015).
18. Hongwei, Z., Fangtian, Y., Hongshang, P. & Huang, S. Energy transfer from Ce^{3+} to Tb^{3+}, Dy^{3+} and Eu^{3+} in $Na_3Y(BO_3)_2$. *J. Rare Earths* **33**, 1051–1055 (2015).
19. Ronda, C. & Meijerink, A. On the mechanism leading to afterglow in Gd_2O_2S:Pr. *Opt. Mater. X* **12**, 100091 (2021).
20. Liu, F., Liang, Y. & Pan, Z. Detection of up-converted persistent luminescence in the near infrared emitted by the $Zn_3Ga_2GeO_8$:Cr^{3+},Yb^{3+},Er^{3+} phosphor. *Phys. Rev. Lett.* **113**, 177401 (2014).
21. Li, Y. et al. A strategy for developing near infrared long-persistent phosphors: taking $MAlO_3$:Mn^{4+},Ge^{4+} (M = La, Gd) as an example. *J. Mater. Chem. C* **2**, 2019–2027 (2014).
22. Pan, Z. et al. Facilitating low-energy activation in the near-infrared persistent luminescent phosphor $Zn_{1+x}Ga_{2-2x}Sn_xO_4$:Cr^{3+} via crystal field strength modulations. *J. Phys. Chem. C* **124**, 8347–8358 (2020).
23. Ivanovskii, A. L., Gubanov, V. A., Kurmaev, E. Z. & Shveikin, G. P. Electronic structure and the chemical bond in non-stoichiometric refractory compounds of transition metals in sub-groups IVa and Va. *Russ. Chem. Rev.* **52**, 395 (1983).
24. Suriyamurthy, N. & Panigrahi, B. Effects of non-stoichiometry and substitution on photoluminescence and afterglow luminescence of $Sr_4Al_{14}O_{25}$:Eu^{2+},Dy^{3+} phosphor. *J. Lumin.* **128**, 1809–1814 (2008).
25. Abdukayum, A., Chen, J.-T., Zhao, Q. & Yan, X.-P. Functional near infrared-emitting Cr^{3+}/Pr^{3+} co-doped zinc gallogermanate persistent luminescent nanoparticles with superlong afterglow for in vivo targeted bioimaging. *J. Am. Chem. Soc.* **135**, 14125–14133 (2013).
26. Aitasalo, T. et al. Persistent luminescence phenomena in materials doped with rare earth ions. *J. Solid State Chem.* **171**, 114–122 (2003).
27. Dorenbos, P. Electronic structure engineering of lanthanide activated materials. *J. Mater. Chem.* **22**, 22344–22349 (2012).
28. Bos, A. J. et al. Study of TL glow curves of YPO_4 double doped with lanthanide ions. *Radiat. Meas.* **46**, 1410–1416 (2011).
29. Duan, H., Dong, Y., Huang, Y., Hu, Y. & Chen, X. The important role of oxygen vacancies in $Sr_2MgSi_2O_7$ phosphor. *Phys. Lett. A* **380**, 1056–1062 (2016).
30. Bessière, A., Lecointre, A., Priolkar, K. & Gourier, D. Role of crystal defects in red long-lasting phosphorescence of $CaMgSi_2O_6$:Mn diopsides. *J. Mater. Chem.* **22**, 19039–19046 (2012).
31. Du, J., Feng, A. & Poelman, D. Temperature dependency of trap-controlled persistent luminescence. *Laser Photon. Rev.* **14**, 2000060 (2020).
32. Ou, X. et al. High-resolution X-ray luminescence extension imaging. *Nature* **590**, 410–415 (2021).
33. Gao, Q. et al. Manipulating trap filling of persistent phosphors upon illumination by using a blue light-emitting diode. *J. Mater. Chem. C* **8**, 6988–6992 (2020).

34. Zhuang, Y. et al. X-ray-charged bright persistent luminescence in $NaYF_4$:Ln^{3+}@ $NaYF_4$ nanoparticles for multidimensional optical information storage. *Light. Sci. Appl.* **10**, 132 (2021).
35. Zhuang, Y., Katayama, Y., Ueda, J. & Tanabe, S. A brief review on red to near-infrared persistent luminescence in transition-metal-activated phosphors. *Opt. Mater.* **36**, 1907–1912 (2014).
36. Li, Y. et al. Folic acid-conjugated chromium(III) doped nanoparticles consisting of mixed oxides of zinc, gallium and tin, and possessing near-infrared and long persistent phosphorescence for targeted imaging of cancer cells. *Microchim. Acta* **182**, 1827–1834 (2015).
37. Katayama, Y., Kayumi, T., Ueda, J. & Tanabe, S. Enhanced persistent red luminescence in Mn^{2+}-doped (Mg,Zn)GeO_3 by electron trap and conduction band engineering. *Opt. Mater.* **79**, 147–151 (2018).
38. Wei, X. et al. Longer and stronger: improving persistent luminescence in size-tuned zinc gallate nanoparticles by alcohol-mediated chromium doping. *ACS Nano* **14**, 12113–12124 (2020).
39. Wu, Y. et al. Near-infrared long-persistent phosphor of $Zn_3Ga_2Ge_2O_{10}$:Cr^{3+} sintered in different atmosphere. *Spectrochim. Acta A* **151**, 385–389 (2015).
40. Luo, H., Cao, J., Li, X., Wang, X. & Peng, M. Topological tailoring of structure and defects to enhance red to near-infrared afterglow from Mn^{2+}-doped germanate photonic glasses. *J. Mater. Chem. C* **6**, 11525–11535 (2018).
41. Qin, X. et al. A novel NIR long phosphorescent phosphor: $SrSnO_3$:Bi^{2+}. *RSC Adv.* **5**, 101347–101352 (2015).
42. Nie, J. et al. Tunable long persistent luminescence in the second near-infrared window via crystal field control. *Sci. Rep.* **7**, 12392 (2017).
43. Eliseeva, S. V. & Bünzli, J.-C. G. Lanthanide luminescence for functional materials and bio-sciences. *Chem. Soc. Rev.* **39**, 189–227 (2010).
44. Rojas-Hernandez, R. E., Rubio-Marcos, F., Rodriguez, M. Á. & Fernandez, J. F. Long lasting phosphors: $SrAl_2O_4$:Eu,Dy as the most studied material. *Renew. Sustain. Energy Rev.* **81**, 2759–2770 (2018).
45. Yu, N., Liu, F., Li, X. & Pan, Z. Near infrared long-persistent phosphorescence in $SrAl_2O_4$:Eu^{2+},Dy^{3+},Er^{3+} phosphors based on persistent energy transfer. *Appl. Phys. Lett.* **95**, 231110 (2009).
46. Xu, J., Murata, D., Katayama, Y., Ueda, J. & Tanabe, S. Cr^{3+}/Er^{3+} co-doped $LaAlO_3$ perovskite phosphor: a near-infrared persistent luminescence probe covering the first and third biological windows. *J. Mater. Chem. B* **5**, 6385–6393 (2017).
47. You, F., Bos, A. J., Shi, Q., Huang, S. & Dorenbos, P. Electron transfer process between Ce^{3+} donor and Yb^{3+} acceptor levels in the bandgap of $Y_3Al_5O_{12}$ (YAG). *J. Condens. Matter Phys.* **23**, 215502 (2011).
48. Xu, J., Tanabe, S., Sontakke, A. D. & Ueda, J. Near-infrared multi-wavelengths long persistent luminescence of Nd^{3+} ion through persistent energy transfer in Ce^{3+}, Cr^{3+} co-doped $Y_3Al_2Ga_3O_{12}$ for the first and second bio-imaging windows. *Appl. Phys. Express* **107**, 081903 (2015).
49. Srivastava, B. B., Gupta, S. K., Mohan, S. & Mao, Y. Molten salt assisted annealing for making colloidal $ZnGa_2O_4$:Cr nanocrystals with high persistent luminescence. *Chem. Eur. J.* **27**, 11398–11405 (2021).
50. Wei, X. et al. Continuous flow synthesis of persistent luminescent chromium-doped zinc gallate nanoparticles. *J. Phys. Chem. Lett.* **12**, 7067–7075 (2021).
51. Fu, L. et al. Enhancement of long-lived luminescence in nanophosphors by surface defect passivation. *Chem. Commun.* **56**, 6660–6663 (2020).
52. Zou, W., Visser, C., Maduro, J. A., Pshenichnikov, M. S. & Hummelen, J. C. Broadband dye-sensitized upconversion of near-infrared light. *Nat. Photon.* **6**, 560–564 (2012).
53. Li, Z. et al. Enhancing rechargeable persistent luminescence via organic dye sensitization. *Angew. Chem. Int. Ed.* **60**, 15886–15890 (2021).
54. Amendola, V., Pilot, R., Frasconi, M., Marago, O. M. & Iatì, M. A. Surface plasmon resonance in gold nanoparticles: a review. *J. Condens. Matter Phys.* **29**, 203002 (2017).
55. Hai, O. et al. Plasma effect: a simple method for improving the persistent luminescence and light response range of persistent luminescent materials. *J. Lumin.* **217**, 116785 (2020).
56. Hai, O. et al. Enhancement of the persistent luminescence of $Sr_2MgSi_2O_7$:Eu^{2+},Dy^{3+} by Cu nanoparticles. *J. Lumin.* **220**, 116965 (2020).
57. Srivastava, B. B., Kuang, A. & Mao, Y. Persistent luminescent sub-10 nm Cr doped $ZnGa_2O_4$ nanoparticles by a biphasic synthesis route. *Chem. Commun.* **51**, 7372–7375 (2015).
58. Zhan-Jun, L., Hong-Wu, Z., Meng, S., Jiang-Shan, S. & Hai-Xia, F. A facile and effective method to prepare long-persistent phosphorescent nanospheres and its potential application for in vivo imaging. *J. Mater. Chem.* **22**, 24713–24720 (2012).
59. Li, Z. et al. In vivo repeatedly charging near-infrared-emitting mesoporous SiO_2/$ZnGa_2O_4$:Cr^{3+} persistent luminescence nanocomposites. *Adv. Sci.* **2**, 1500001 (2015).
60. Liu, Y. et al. Mesoporous TiO_2 mesocrystals: remarkable defects-induced crystallite-interface reactivity and their in situ conversion to single crystals. *ACS Cent. Sci.* **1**, 400–408 (2015).
61. Baziulyte-Paulaviciene, D., Traskina, N., Vargalis, R., Katelnikovas, A. & Sakirzanovas, S. Thermal decomposition synthesis of Er^{3+}-activated $NaYbF_4$ upconverting microparticles for optical temperature sensing. *J. Lumin.* **215**, 116672 (2019).
62. Hu, Y. et al. X-ray-excited super-long green persistent luminescence from Tb^{3+} monodoped β-$NaYF_4$. *J. Phys. Chem. C* **124**, 24940–24948 (2020).
63. Xue, Z. et al. X-ray-activated near-infrared persistent luminescent probe for deep-tissue and renewable in vivo bioimaging. *ACS Appl. Mater. Interfaces* **9**, 22132–22142 (2017).
64. Relvas, M. et al. Trends in Cr^{3+} red emissions from $ZnGa_2O_4$ nanostructures produced by pulsed laser ablation in a liquid medium. *J. Phys. Chem. Solids* **129**, 413–423 (2019).
65. Maldiney, T. et al. In vivo optical imaging with rare earth doped $Ca_2Si_5N_8$ persistent luminescence nanoparticles. *Opt. Mater. Express* **2**, 261–268 (2012).
66. Li, Y.-J. & Yan, X.-P. Synthesis of functionalized triple-doped zinc gallogermanate nanoparticles with superlong near-infrared persistent luminescence for long-term orally administrated bioimaging. *Nanoscale* **8**, 14965–14970 (2016).
67. Maldiney, T. et al. The in vivo activation of persistent nanophosphors for optical imaging of vascularization, tumours and grafted cells. *Nat. Mater.* **13**, 418–426 (2014).
68. Wu, B.-Y., Wang, H.-F., Chen, J.-T. & Yan, X.-P. Fluorescence resonance energy transfer inhibition assay for α-fetoprotein excreted during cancer cell growth using functionalized persistent luminescence nanoparticles. *J. Am. Chem. Soc.* **133**, 686–688 (2010).
69. Chen, N. et al. Real-time monitoring of dynamic microbial Fe(III) respiration metabolism with a living cell-compatible electron-sensing probe. *Angew. Chem. Int. Ed.* **61**, e202115572 (2022).
70. Wu, B.-Y. & Yan, X.-P. Bioconjugated persistent luminescence nanoparticles for Föster resonance energy transfer immunoassay of prostate specific antigen in serum and cell extracts without in situ excitation. *Chem. Commun.* **51**, 3903–3906 (2015).

71. Healy, D. A., Hayes, C. J., Leonard, P., McKenna, L. & O'Kennedy, R. Biosensor developments: application to prostate-specific antigen detection. *Trends Biotechnol.* **25**, 125–131 (2007).
72. Xue, Z. et al. A 980 nm laser-activated upconverted persistent probe for NIR-to-NIR rechargeable in vivo bioimaging. *Nanoscale* **9**, 7276–7283 (2017).
73. Zhou, Z. et al. Rechargeable and LED-activated $ZnGa_2O_4$:Cr^{3+} near-infrared persistent luminescence nanoprobes for background-free biodetection. *Nanoscale* **9**, 6846–6853 (2017).
74. Zou, R. et al. Silica shell-assisted synthetic route for mono-disperse persistent nanophosphors with enhanced in vivo recharged near-infrared persistent luminescence. *Nano Res.* **10**, 2070–2082 (2017).
75. Maldiney, T. et al. Effect of core diameter, surface coating, and PEG chain length on the biodistribution of persistent luminescence nanoparticles in mice. *ACS Nano* **5**, 854–862 (2011).
76. Chen, L.-J., Yang, C.-X. & Yan, X.-P. Liposome-coated persistent luminescence nanoparticles as luminescence trackable drug carrier for chemotherapy. *Anal. Chem.* **89**, 6936–6939 (2017).
77. Sun, S.-K. et al. Turning solid into gel for high-efficient persistent luminescence-sensitized photodynamic therapy. *Biomaterials* **218**, 119328 (2019).
78. Abdurahman, R., Yang, C.-X. & Yan, X.-P. Conjugation of a photosensitizer to near infrared light renewable persistent luminescence nanoparticles for photodynamic therapy. *Chem. Commun.* **52**, 13303–13306 (2016).
79. Ma, Q. et al. Near-infrared-light-mediated high-throughput information encryption based on the inkjet printing of upconversion nanoparticles. *Inorg. Chem. Front.* **4**, 1166–1172 (2017).
80. Kim, S.-J., Choi, M., Hong, G. & Hahn, S. K. Controlled afterglow luminescent particles for photochemical tissue bonding. *Light Sci. Appl.* **11**, 314 (2022).
81. Alkauskas, A., McCluskey, M. D. & Van de Walle, C. G. Tutorial: defects in semiconductors—combining experiment and theory. *Int. J. Appl. Phys.* **119**, 181101 (2016).
82. Li, H. et al. Theory-guided defect tuning through topochemical reactions for accelerated discovery of UVC persistent phosphors. *Adv. Opt. Mater.* **8**, 1901727 (2020).
83. Liu, Z., Zhu, D., Raju, L. & Cai, W. Tackling photonic inverse design with machine learning. *Adv. Sci.* **8**, 2002923 (2021).
84. Poon, W. et al. Elimination pathways of nanoparticles. *ACS Nano* **13**, 5785–5798 (2019).
85. de Chermont, Q. l. M. et al. Nanoprobes with near-infrared persistent luminescence for in vivo imaging. *Proc. Natl Acad. Sci. USA* **104**, 9266–9271 (2007).
86. Teston, E. et al. Non-aqueous sol–gel synthesis of ultra small persistent luminescence nanoparticles for near-infrared in vivo imaging. *Chem. Eur. J.* **21**, 7350–7354 (2015).
87. Zou, R. et al. Magnetic-NIR persistent luminescent dual-modal ZGOCS@MSNs@Gd_2O_3 core–shell nanoprobes for in vivo imaging. *Chem. Mater.* **29**, 3938–3946 (2017).
88. Wang, J., Li, J., Yu, J., Zhang, H. & Zhang, B. Large hollow cavity luminous nanoparticles with near-infrared persistent luminescence and tunable sizes for tumor afterglow imaging and chemo-/photodynamic therapies. *ACS Nano* **12**, 4246–4258 (2018).
89. Gao, Y.-F. et al. Large-pore mesoporous-silica-assisted synthesis of high-performance $ZnGa_2O_4$:Cr^{3+}/Sn^{4+}@MSNs multifunctional nanoplatform with optimized optical probe mass ratio and superior residual pore volume for improved bioimaging and drug delivery. *Chem. Eng. Sci.* **420**, 130021 (2021).
90. Lin, Y. et al. Multiple emission bands NIR-persistent luminescence mSiO_2@$Zn_{0.6}Ca_{0.4}Ga_2O_4$:Cr^{3+},Yb^{3+} nanoparticles for biological applications. *J. Mater. Chem. B* **9**, 1131–1137 (2021).
91. Jiang, R. et al. X-ray/red-light excited ZGGO:Cr,Nd nanoprobes for NIR-I/II afterglow imaging. *Dalton Trans.* **49**, 6074–6083 (2020).
92. Ma, C. et al. The second near-infrared window persistent luminescence for anti-counterfeiting application. *Cryst. Growth Des.* **20**, 1859–1867 (2020).
93. Zheng, S. et al. X-ray recharged long afterglow luminescent nanoparticles $MgGeO_3$:Mn^{2+},Yb^{3+},Li^{+} in the first and second biological windows for long-term bioimaging. *Nanoscale* **12**, 14037–14046 (2020).
94. Wu, L. et al. Synthesis and optical properties of a $Y_3(Al/Ga)_5O_{12}$:Ce^{3+},Cr^{3+},Nd^{3+} persistent luminescence nanophosphor: a promising near-infrared-II nanoprobe for biological applications. *Nanoscale* **12**, 14180–14187 (2020).
95. Liu, B.-M. et al. Low-dose X-ray-stimulated $LaGaO_3$:Sb,Cr near-infrared persistent luminescence nanoparticles for deep-tissue and renewable in vivo bioimaging. *Chem. Eng. Sci.* **404**, 127133 (2021).
96. Chen, X. et al. Trap energy upconversion-like near-infrared to near-infrared light rejuvenateable persistent luminescence. *Adv. Mater.* **33**, 2008722 (2021).
97. Li, J. et al. Porous $GdAlO_3$:Cr^{3+},Sm^{3+} drug carrier for real-time long afterglow and magnetic resonance dual-mode imaging. *J. Lumin.* **199**, 363–371 (2018).
98. Resch-Genger, U., Grabolle, M., Cavaliere-Jaricot, S., Nitschke, R. & Nann, T. Quantum dots versus organic dyes as fluorescent labels. *Nat. Methods* **5**, 763–775 (2008).
99. Zimmer, M. Green fluorescent protein (GFP): applications, structure, and related photophysical behavior. *Chem. Rev.* **102**, 759–782 (2002).
100. Chalfie, M. & Kain, S. R. *Green Fluorescent Protein: Properties, Applications and Protocols* (John Wiley & Sons, 2005).
101. Xu, Y. et al. Tuning molecular aggregation to achieve highly bright AIE dots for NIR-II fluorescence imaging and NIR-I photoacoustic imaging. *Chem. Sci.* **11**, 8157–8166 (2020).
102. Liu, H. et al. AIE bioconjugates for biomedical applications. *Adv. Opt. Mater.* **8**, 2000162 (2020).
103. Xu, W., Wang, D. & Tang, B. Z. NIR-II AIEgens: a win–win integration towards bioapplications. *Angew. Chem. Int. Ed.* **133**, 7552–7563 (2021).
104. Zhi, J., Zhou, Q., Shi, H., An, Z. & Huang, W. Organic room temperature phosphorescence materials for biomedical applications. *Chem. Asian J.* **15**, 947–957 (2020).
105. Lim, S. Y., Shen, W. & Gao, Z. Carbon quantum dots and their applications. *Chem. Soc. Rev.* **44**, 362–381 (2015).
106. Jamieson, T. et al. Biological applications of quantum dots. *Biomaterials* **28**, 4717–4732 (2007).
107. Smith, A. M., Duan, H., Mohs, A. M. & Nie, S. Bioconjugated quantum dots for in vivo molecular and cellular imaging. *Adv. Drug Deliv. Rev.* **60**, 1226–1240 (2008).
108. Torelli, M. D., Nunn, N. A. & Shenderova, O. A. A perspective on fluorescent nanodiamond bioimaging. *Small* **15**, 1902151 (2019).
109. Claveau, S., Bertrand, J.-R. & Treussart, F. Fluorescent nanodiamond applications for cellular process sensing and cell tracking. *Micromachines* **9**, 247 (2018).
110. Wang, L., Draz, M. S., Wang, W., Liao, G. & Xu, Y. The quality of in vivo upconversion fluorescence signals inside different anatomic structures. *J. Biomed. Nanotechnol.* **11**, 325–333 (2015).
111. Wang, J., Ma, Q., Wang, Y., Shen, H. & Yuan, Q. Recent progress in biomedical applications of persistent luminescence nanoparticles. *Nanoscale* **9**, 6204–6218 (2017).

Acknowledgements

This work was supported by the Agency for Science, Technology and Research (grant no. A1983c0038); the National Research Foundation, the Prime Minister's Office of Singapore under its Investigatorship

Programme (award no. NRF-NRFI05-2019-0003); the National Natural Science Foundation of China (nos 10804099, 21804119, 21771135 and 21871071); the Key Projects of Zhejiang Natural Science Foundation (project no. LZ18B050002); and the China Scholarship Council (no. 201408330001).

Author contributions

L.L. and Z.P. wrote this review, and X.L. edited it. J.C., K.S. and X.Q. assisted in the preparation of the manuscript.

Competing interests

The authors declare no competing interests.

Additional information

Correspondence should be addressed to Zaifa Pan or Xiaogang Liu.

Peer review information *Nature Materials* thanks the anonymous reviewers for their contribution to the peer review of this work.